Materials Science & Engineering A 682 (2017) 354–358

Contents lists available at ScienceDirect

Materials Science & Engineering A

journal homepage: www.elsevier.com/locate/msea

Short communication

Room temperature deformation of LPSO structures by non-basal slip

Ran Chen[a,b], Stefanie Sandlöbes[b,c,**], Xiaoqin Zeng[a,*], Dejiang Li[a], Sandra Korte-Kerzel[c], Dierk Raabe[b]

[a] The State Key Laboratory of Metal Matrix Composites, Shanghai Jiao Tong University, 200240 Shanghai, PR China
[b] Max-Planck-Institut für Eisenforschung, Max-Planck-Str. 1, 40237 Düsseldorf, Germany
[c] Institute of Physical Metallurgy and Metal Physics, RWTH Aachen University, 52056 Aachen, Germany

ARTICLE INFO

Keywords:
Mg-LPSO alloy
Deformation mechanisms
Dislocations
Transmission electron microscopy

ABSTRACT

We investigated the deformation mechanisms of long period stacking ordered (LPSO) structures in an extruded $Mg_{97}Y_2Zn_1$ (at%) alloy. Tensile deformation was performed in such a way that basal slip and kink band formation were inhibited. Slip trace analysis and transmission electron microscopy reveal a predominant activity of non-basal < a > slip.

1. Introduction

Magnesium alloys are attractive structural materials due to their low density, high specific strength and good recyclability [1]. However, due to the hexagonal crystal structure of Mg and the related crystallographic anisotropy, only a limited set of slip systems is available resulting in poor room temperature ductility [2,3]. Recently Mg-Y-Zn and Mg-Zn-RE alloys containing long period stacking ordered (LPSO) structures have been reported to possess both high strength and good toughness [4–10]. This excellent mechanical performance has been reported to be related to the presence of LPSO structures, however, the underlying mechanisms for the concomitant increase of strength and toughness are not fully understood [5–11]. LPSO structures are chemically and structurally ordered where RE/Y and Zn atoms occupy Mg positions on neighboring {0001} planes. They share the {0001} basal plane of Mg but are stacking ordered along the c-axis, resulting in stacking periods such as 10H, 14H, 18R and 24R [12–15]. For pure Mg and most magnesium alloys, $\{0001\}\langle 11\bar{2}0\rangle$ basal < a > dislocation slip and $\{10\bar{1}2\}\langle 10\bar{1}\bar{1}\rangle$ twinning are the two predominant deformation mechanisms at room temperature [2,3,16]. However, it has been shown for LPSO structures that twinning is strongly inhibited due to the long stacking periodicity and ordering of RE and Zn atoms [17,18]. Instead, the formation of kink bands has been reported during deformation of LPSO grains, which - together with basal dislocation slip - effectively carries the strain in LPSO structures at room temperature [6–9,11,18–23]. Previous studies also suggest only limited activity of non-basal slip which has been observed only in regions with high local stress concentrations such as adjacent to kink bands during room temperature deformation of LPSO grains [19–22]. Generally, the activation of deformation systems strongly depends on the crystallographic texture and the loading direction [24].

Therefore, this study aims at investigating the active deformation mechanisms in LPSO structures at room temperature under conditions where both, basal slip and kink band formation, are restricted. To this end we investigated the room temperature tensile deformation behavior of an extruded $Mg_{97}Y_2Zn_1$ (at%) alloy which was deformed by tensile loading parallel to the basal planes, hence, restricting the activation of basal slip and kink band formation. By combined slip trace analysis, electron backscatter diffraction (EBSD) and transmission electron microscopy (TEM) we observed a surprising prevalence of non-basal < a > slip in the LPSO structures.

2. Experimental methods

The $Mg_{97}Y_2Zn_1$ (at%) alloy investigated was prepared by electric resistance melting and gravity casting. The ingot was homogenized at 803 K for 30 h and then extruded at 623 K with a reduction rate of 9.97:1 and a ram speed of 2.5 mm s^{-1}. A subsequent heat treatment followed by water quenching was conducted at 773 K for 48 h to release the high strain induced by the extrusion process. After mechanical grinding and polishing, scanning electron microscopy (SEM) and EBSD mapping were applied to examine the microstructure and the crystallographic texture of the longitudinal section of the annealed extrusion bar.

Tensile test samples with gauge dimensions of 4 mm×2 mm×1 mm were prepared along the extrusion direction (ED) by electric discharge

* Corresponding author at: The State Key Laboratory of Metal Matrix Composites, Shanghai Jiao Tong University, 200240 Shanghai, PR China.
** Corresponding author at: Institute of Physical Metallurgy and Metal Physics, RWTH Aachen University, 52056 Aachen, Germany.
E-mail addresses: sandloebes@imm.rwth-aachen.de (S. Sandlöbes), xqzeng@sjtu.edu.cn (X. Zeng).

http://dx.doi.org/10.1016/j.msea.2016.11.056
Received 28 June 2016; Received in revised form 16 November 2016; Accepted 17 November 2016
Available online 18 November 2016
0921-5093/

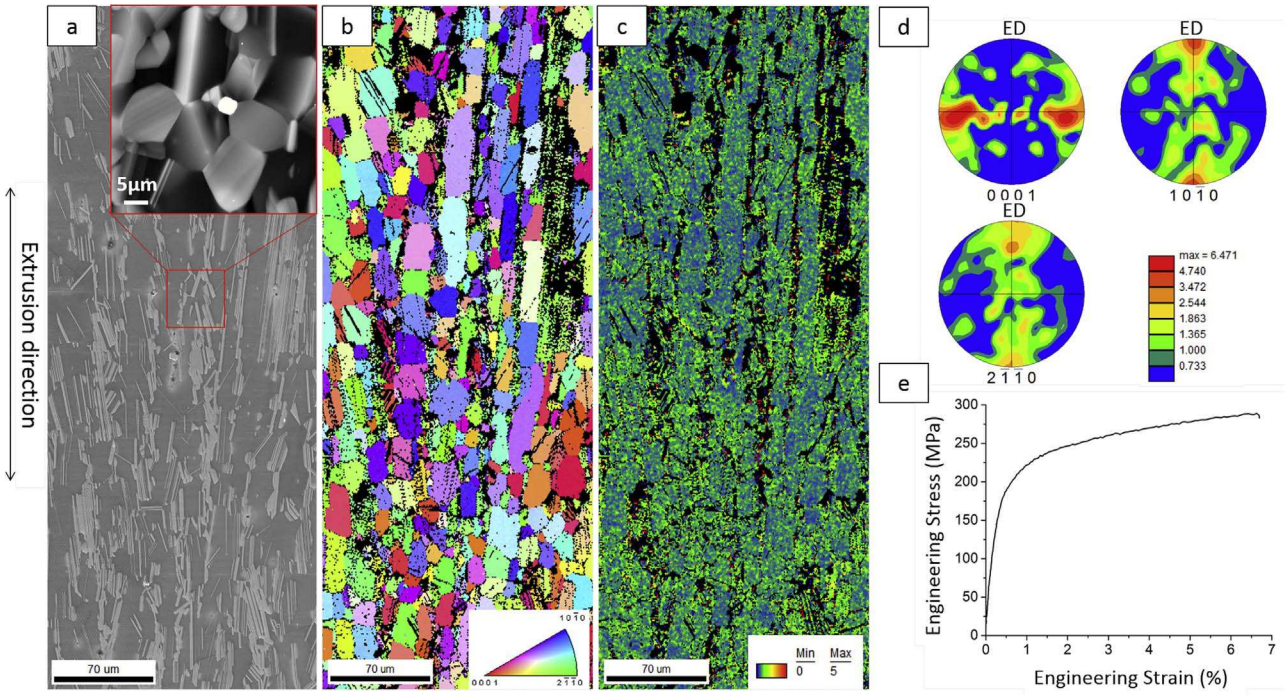

Fig. 1. (a) Secondary electron image, (b) inverse pole figure map of α-Mg and LPSO structure, (c) kernel average misorientation map of α-Mg and LPSO structure, (d) pole figures of the longitudinal sample section representing equally the texture of both microstructural constituents, α-Mg and LPSO structures, due to the $\{0001\}_{LPSO}//\{0001\}_{\alpha\text{-}Mg}$ orientation relationship between α-Mg and LPSO; the inset in (a) shows an enlarged backscattered electron micrograph of the LPSO structures, (e) engineering stress-strain curve of tensile test up to 6.7% strain.

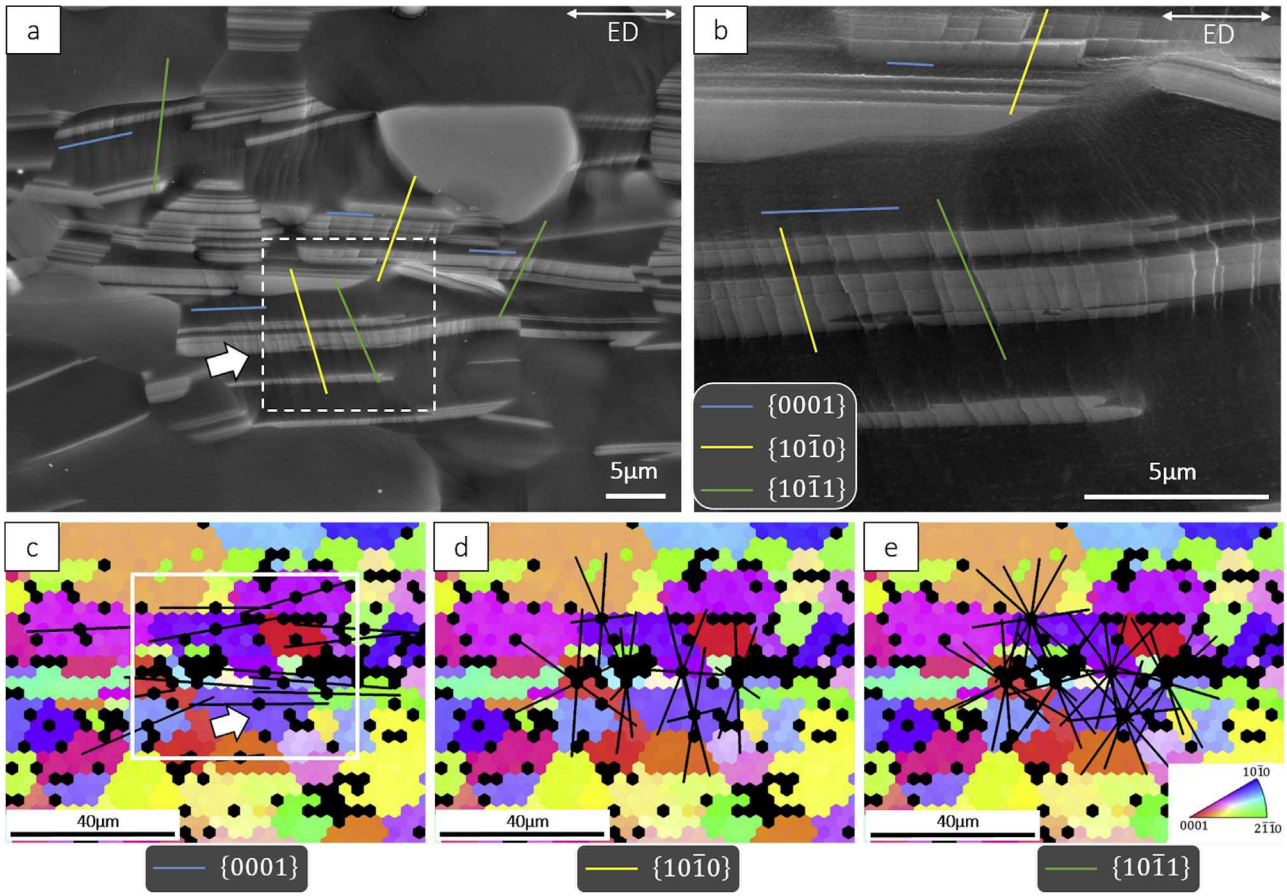

Fig. 2. (a) Secondary electron image of typical slip traces in a sample deformed in tension to 6.7% strain, (b) higher magnification image of the area marked by the rectangle in (a). (c)–(e) Inverse pole figure maps where the {0001}, {10$\bar{1}$0} and {10$\bar{1}$1} plane traces are marked; the position of the micrograph in (a) is marked by the rectangular in (c).

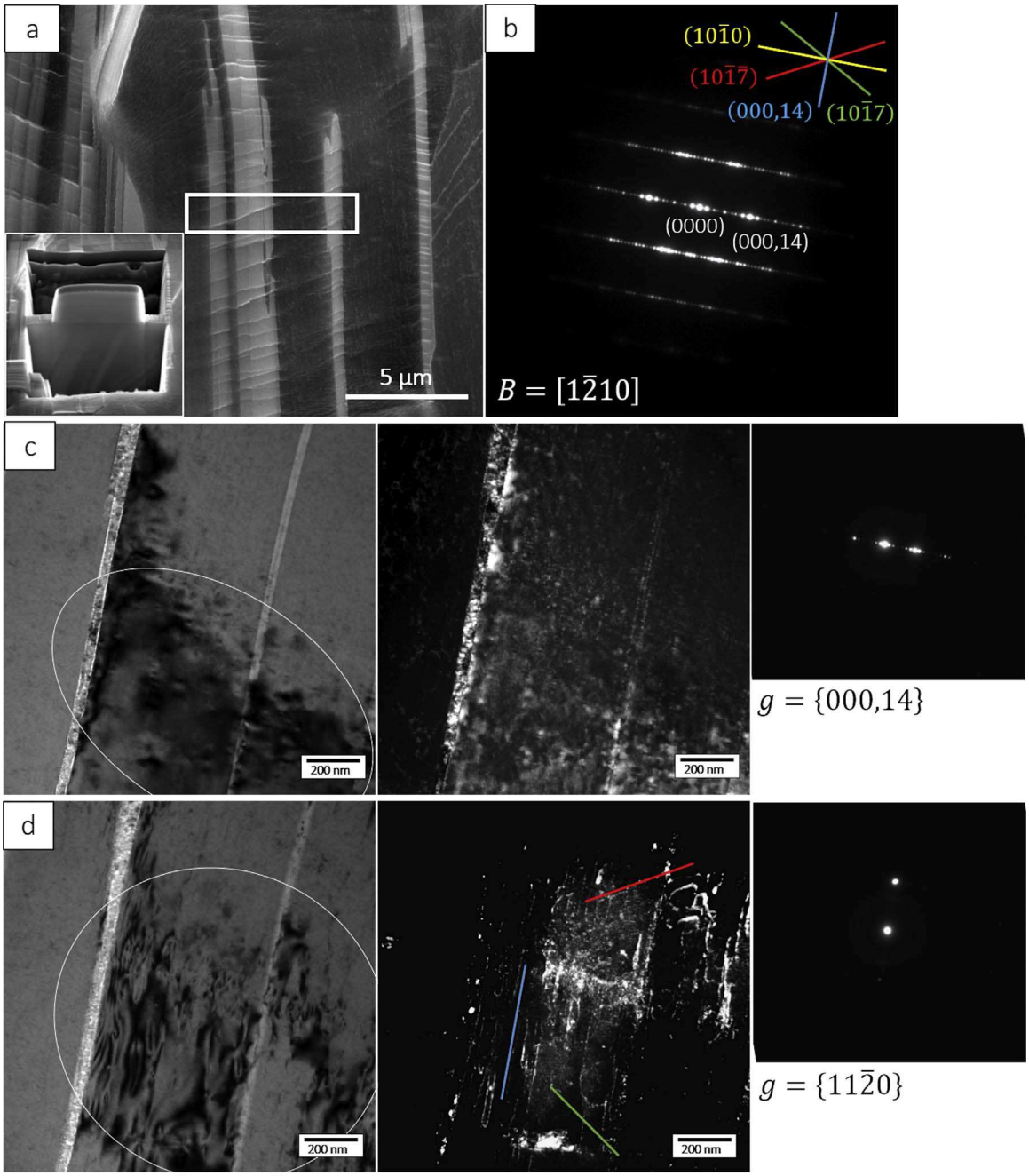

Fig. 3. (a) Secondary electron image showing the position of the TEM lamellar analyzed in (b)–(d). (b) Selected area diffraction pattern obtained from the largest LPSO plate in (a). The electron beam is parallel to B=$\{11\bar{2}0\}_{LPSO}$. (c), (d) TEM bright field and weak beam dark field images under $\vec{g}=\{000,\ 14\}_{LPSO}$ and $\vec{g}=\{11\bar{2}0\}_{LPSO}$, the regions of the sample which fulfil exact 2-beam conditions are marked by white ellipses; B: zone axis, $\vec{g}$: diffraction vector. The images in (b)–(d) originate from the same position.

machining and subsequent mechanical grinding and polishing on one surface of the specimens. Room temperature tensile tests along the ED were performed using a KAMMRATH & WEISS (Dortmund, Germany) stage imposing an initial strain rate of $1.25 \times 10^{-3}\ s^{-1}$. The test was stopped at an engineering strain of 6.7%. EBSD mapping and secondary electron (SE) observations of the gauge area were conducted both, prior to and after tensile deformation. TEM samples were prepared site-specifically using a focused ion beam instrument (FIB, FEI Helios NanoLab 600) on areas with prevalent $\{10\bar{1}1\}$ slip traces. TEM observations were performed on a CM20 microscope operated at 200 kV.

According to the study of Hess and Barrett [24], kink band formation is facilitated by compression parallel to the basal plane of hexagonal Zn and, hence, likely to be activated upon compressive loading along the basal planes. In contrast, tensile loading along the basal planes is unfavorable for the formation of kink bands. Therefore, different from studies which revealed kink band formation by compression parallel to the basal planes [19,20], we imposed tensile load along ED, i.e. the tensile direction is aligned parallel to the basal planes. Furthermore, grains with a $\langle 1\bar{1}00\rangle$ texture have low Schmid factors for basal < a > slip when deformed parallel to the basal planes. Hence, the reported two predominant deformation modes of LPSO grains, namely basal < a > slip and kink band formation, were both supposed to be suppressed in our experiments.

3. Results and discussion

In the micrographs in Fig. 1(a) the LPSO phase shows brighter

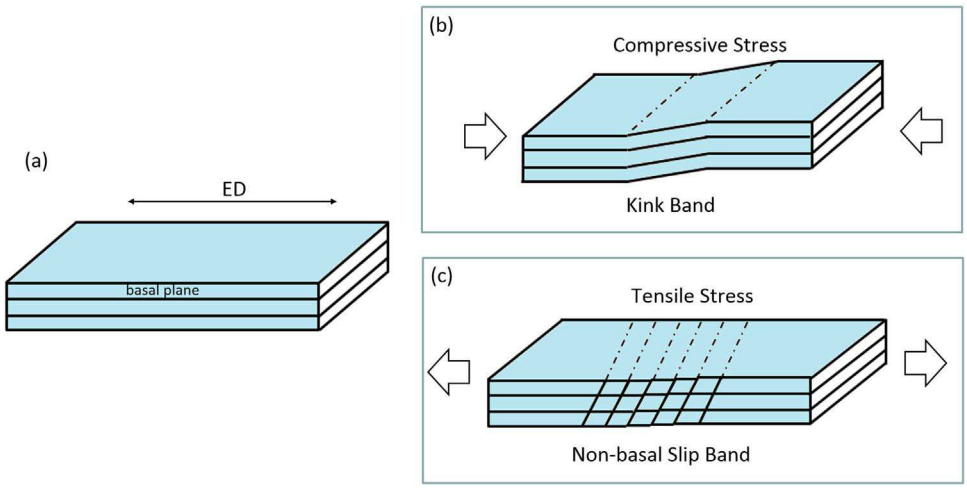

Fig. 4. (a) LPSO platelets in an extruded Mg-LPSO alloy with a $\langle 1\bar{1}00\rangle$ texture. Under compressive loading, i.e. loading direction parallel to the basal plane, the predominant deformation mechanism is the formation of kink bands (b), while under tensile loading non-basal < a > slip is predominantly activated (c).

contrast than the α-Mg grains. As revealed in the micrographs, most of the LPSO grains have a platelet-like morphology elongated along the ED. The inverse pole figure (IPF), Fig. 1(b), and first nearest-neighbor kernel average misorientation (KAM), Fig. 1(c), maps reveal only low (≤1°) in-grain misorientations indicating that the microstructure contains mainly recrystallized grains while only a small fraction of deformed grains (~8% area fraction) remained. The pole figure (PF) maps in Fig. 1(d) display a $\langle 1\bar{1}00\rangle$ texture characterized by the alignment of the {0001} basal planes parallel to the ED, revealing that the $\langle 1\bar{1}00\rangle$ texture, which is known to form during extrusion [6], prevails after annealing at 773 K for 48 h. Fig. 1(e) shows the engineering stress-strain curve up to a strain of 6.7%.

SEM-EBSD slip trace analysis of the active glide planes was performed after tensile deformation on the polished surface considering all crystallographically possible glide planes, including the second order pyramidal planes ($\{11\bar{2}2\}$). Numerous surface steps which crystallographically match to slip planes in LPSO structures were observed but no kink band formation, Fig. 2(a) and (b). Fig. 2(c)–(e) shows IPF maps of the same area as the SEM images in Fig. 2(a) and (b) where the calculated plane traces of the observed active {0001}, $\{10\bar{1}0\}$ and $\{10\bar{1}1\}$ glide planes are marked. Due to the high ordering and crystallographic similarity of hcp α-Mg and LPSO structures, the platelet-like LPSO structures were partly indexed as hcp α-Mg using EBSD. However, the observed orientation relationship $\{0001\}_{LPSO}//\{0001\}_{\alpha\text{-}Mg}$ [6,12,23,25] between the platelet-like LPSO structures and the α-Mg matrix and TEM observations on site-specifically prepared samples confirm correct identification of the crystallographic orientations using EBSD. Almost all slip traces observed after 6.7% tensile deformation in LPSO structures correspond to non-basal planes, indicating that non-basal dislocation slip may be activated in LPSO under the applied loading conditions. Most slip traces displayed in Fig. 2(a) were identified to pertain to the $\{10\bar{1}0\}$ prismatic and $\{10\bar{1}1\}$ first order pyramidal planes (corresponding to $\{10\bar{1}0\}$ and $\{10\bar{1}\bar{7}\}$ planes for 14H hexagonal lattice). Similarly activated slip traces were found in the entire sample after tensile deformation to 6.7% engineering strain. Further, the observed non-basal slip traces have a wavy appearance, Fig. 2(b), indicating either cross-slip or the interaction with dislocations on other glide planes.

Analysis of the dislocations inside the LPSO structure was conducted according to the $\vec{g}\bullet\vec{b}$ analysis ($\vec{g}$: diffraction vector; $\vec{b}$: Burgers vector). The diffraction pattern taken along the zone axis $B=[11\bar{2}0]_{LPSO}$ are shown in Fig. 3(b) indicating that the LPSO structure is of 14H stacking type. Fig. 3(c) and (d) shows TEM bright field (BF) and weak beam dark field (WBDF) images together with the corresponding selected area diffraction patterns (SADP) for $\vec{g}=\{000,14\}_{LPSO}$ and $\vec{g}=\{11\bar{2}0\}_{LPSO}$. Under $\vec{g}=\{000,14\}_{LPSO}$ only dislocations with a < c > -component give contrast indicating that dislocations with a < c > -component are present at the interface between LPSO and α-Mg, but no dislocations with a < c > -component are observed inside the LPSO structure. Fig. 3(d) shows the same area with $\vec{g}=\{11\bar{2}0\}_{LPSO}$ giving contrast only from dislocations with an < a > -component, revealing that the observed dislocations are of < a > type. According to the plane traces illustrated in Fig. 3(d), < a > dislocations on basal $(000,14)_{LPSO}$, first order pyramidal $(10\bar{1}7)_{LPSO}$ and $(10\bar{1}\bar{7})_{LPSO}$ planes are present. Therefore, it is reasonable to conclude that the observed non-basal slip traces in the LPSO structure arise from the slip of < a > dislocations on $(10\bar{1}7)_{LPSO}$ and $(10\bar{1}\bar{7})_{LPSO}$ non-basal planes. Furthermore, nearly all observed dislocations have segments on both non-basal and basal planes. This indicates either the cross-slip of basal < a > dislocations or the interaction of basal < a > and non-basal < a > dislocations, which is also evident from the wavy appearance of slip traces in Fig. 2(b).

These results show that non-basal < a > slip can be activated at ambient temperatures in LPSO structures when basal < a > slip is inhibited due to a low Schmid factor. In the present study, the Schmid factors for $\{0001\}\langle 1\bar{2}10\rangle$, $\{10\bar{1}0\}\langle 1\bar{2}10\rangle$ and $\{10\bar{1}1\}\langle 1\bar{2}10\rangle$ slip systems of the grain marked with a white arrow in Fig. 2(c), are 0.01, 0.47 and 0.42, respectively. Although the exact critical resolved shear stress (CRSS) values of the different slip systems in the LPSO structure remain unknown, Hutchinson et al. [26] reported that the effective CRSS ratio of non-basal < a > to basal < a > slip significantly decreases in polycrystalline samples due to more complex stress states in polycrystalline aggregates. The activation of non-basal slip in LPSO structures has also been shown by Hagihara et al. [19,20] who observed non-basal < a > slip locally in conjunction with kink boundaries in the LPSO structures of an extruded Mg-LPSO alloy deformed at room temperature. By applying tensile loading parallel to the basal planes, we observed considerable non-basal < a > slip activated at room temperature, however, no kink band formation was observed.

Fig. 4 shows a schematic model of the activation of deformation modes and the tension-compression asymmetry of kink band formation in the present study. Loading parallel to the basal planes renders basal dislocation slip energetically unfavorable, Fig. 4(a). Under compressive load the LPSO structure is likely to deform by the formation of kink bands to accommodate the decrease in spacing between the two sites of the LPSO platelet [7,19–21], Fig. 4(b). In the present study it was shown that tensile loading parallel to the basal planes activates non-basal < a > slip to accommodate the tensile strain in LPSO platelets, Fig. 4(c). A further aspect which facilitates non-basal slip rather than the formation of kink bands is the fact that most LPSO

platelets are embedded as isolated islands in the Mg matrix, see Fig. 1(a). Hence, the formation of kink bands is impeded by the resistance to accommodate the strain in the Mg matrix.

4. Conclusions

We investigated the deformation mechanisms in an extruded Mg-LPSO alloy with $\langle 1\bar{1}00\rangle$ texture. Tensile deformation at room temperature was conducted parallel to the extrusion direction to suppress basal dislocation slip and kink band formation by controlling the Schmid factor and the loading direction. EBSD-assisted slip trace analysis revealed predominant slip traces on prismatic and first-order pyramidal planes in the LPSO structure. TEM analysis on site specifically prepared specimens confirmed < a > dislocation slip on non-basal planes. This activation of non-basal < a > slip is assumed to be caused by a high Schmid factor for non-basal < a > slip and the inhibition of basal < a > slip and kink band formation.

Prime novelty statement

We performed tensile tests with the loading direction parallel to the basal planes of an extruded Mg-LPSO alloy to inhibit basal slip and kink band formation. Combined EBSD-based slip trace analysis and TEM $\vec{g}\bullet\vec{b}$ analysis of the active deformation mechanisms confirmed the activity of non-basal < a > slip in 14H LPSO structure as a predominant deformation mechanism. These findings reveal the ability to activate non-basal deformation mechanisms in highly ordered LPSO structures and, hence, might enable future microstructure design of Mg-LPSO alloy with tailored mechanical properties.

Acknowledgement

This work was supported by the National Natural Science Foundation of China (Nos. 51301107 and 51474149). The first author, R.C., gratefully acknowledges funding by the China Scholarship Council (CSC) grant No 201406230178.

References

[1] Y. Kojima, Project of platform science and technology for advanced magnesium alloys, Mater. Trans. 42 (2001) 1154–1159.
[2] M.R. Barnett, Twinning and the ductility of magnesium alloys: part I: “tension” twins, Mater. Sci. Eng.: A 464 (2007) 1–7.
[3] S.-G. Hong, S.H. Park, C.S. Lee, Role of {10–12} twinning characteristics in the deformation behavior of a polycrystalline magnesium alloy, Acta Mater. 58 (2010) 5873–5885.
[4] Y. Kawamura, K. Hayashi, A. Inoue, T. Masumoto, Rapidly solidified powder metallurgy $Mg_{97}Zn_1Y_2$ alloys with excellent tensile yield strength above 600 MPa, Mater. Trans. 42 (2001) 1172–1176.
[5] E. Abe, Y. Kawamura, K. Hayashi, A. Inoue, Long-period ordered structure in a high-strength nanocrystalline Mg-1 at% Zn-2 at% Y alloy studied by atomic-resolution Z-contrast STEM, Acta Mater. 50 (2002) 3845–3857.
[6] K. Hagihara, A. Kinoshita, Y. Sugino, M. Yamasaki, Y. Kawamura, H.Y. Yasuda, Y. Umakoshi, Effect of long-period stacking ordered phase on mechanical properties of $Mg_{97}Zn_1Y_2$ extruded alloy, Acta Mater. 58 (2010) 6282–6293.
[7] X.H. Shao, Z.Q. Yang, X.L. Ma, Strengthening and toughening mechanisms in Mg–Zn–Y alloy with a long period stacking ordered structure, Acta Mater. 58 (2010) 4760–4771.
[8] M. Yamasaki, T. Anan, S. Yoshimoto, Y. Kawamura, Mechanical properties of warm-extruded Mg-Zn-Gd alloy with coherent 14H long periodic stacking ordered structure precipitate, Scr. Mater. 53 (2005) 799–803.
[9] Y. Kawamura, M. Yamasaki, Formation and mechanical properties of $Mg_{97}Zn_1RE_2$ alloys with long-period stacking ordered structure, Mater. Trans. 48 (2007) 2986–2992.
[10] M. Yamasaki, K. Hashimoto, K. Hagihara, Y. Kawamura, Effect of multimodal microstructure evolution on mechanical properties of Mg–Zn–Y extruded alloy, Acta Mater. 59 (2011) 3646–3658.
[11] J.-K. Kim, S. Sandlöbes, D. Raabe, On the room temperature deformation mechanisms of a Mg–Y–Zn alloy with long-period-stacking-ordered structures, Acta Mater. 82 (2015) 414–423.
[12] Y.M. Zhu, A.J. Morton, J.F. Nie, The 18R and 14H long-period stacking ordered structures in Mg–Y–Zn alloys, Acta Mater. 58 (2010) 2936–2947.
[13] Y.M. Zhu, A.J. Morton, J.F. Nie, Growth and transformation mechanisms of 18R and 14H in Mg–Y–Zn alloys, Acta Mater. 60 (2012) 6562–6572.
[14] M. Matsuda, S. Ii, Y. Kawamura, Y. Ikuhara, M. Nishida, Variation of long-period stacking order structures in rapidly solidified $Mg_{97}Zn_1Y_2$alloy, Mater. Sci. Eng.: A 393 (2005) 269–274.
[15] D. Egusa, E. Abe, The structure of long period stacking/order Mg–Zn–RE phases with extended non-stoichiometry ranges, Acta Mater. 60 (2012) 166–178.
[16] M.R. Barnett, Z. Keshavarz, A.G. Beer, X. Ma, Non-Schmid behaviour during secondary twinning in a polycrystalline magnesium alloy, Acta Mater. 56 (2008) 5–15.
[17] H. Gao, K.-I. Ikeda, T. Morikawa, K. Higashida, H. Nakashima, Analysis of kink boundaries in deformed synchronized long-period stacking ordered magnesium alloys, Mater. Lett. 146 (2015) 30–33.
[18] M. Yamasaki, K. Hagihara, S.-I. Inoue, J.P. Hadorn, Y. Kawamura, Crystallographic classification of kink bands in an extruded Mg-Zn-Y alloy using intragranular misorientation axis analysis, Acta Mater. 61 (2013) 2065–2076.
[19] K. Hagihara, Y. Fukusumi, M. Yamasaki, T. Nakano, Y. Kawamura, Non-basal slip systems operative in $Mg_{12}ZnY$ long-period stacking ordered (LPSO) phase with 18R and 14H structures, Mater. Trans. 54 (2013) 693–697.
[20] K. Hagihara, A. Kinoshita, Y. Sugino, M. Yamasaki, Y. Kawamura, H.Y. Yasuda, Y. Umakoshi, Plastic deformation behavior of $Mg_{89}Zn_4Y_7$ extruded alloy composed of long-period stacking ordered phase, Intermetallics 18 (2010) 1079–1085.
[21] K. Hagihara, N. Yokotani, Y. Umakoshi, Plastic deformation behavior of $Mg_{12}YZn$ with 18R long-period stacking ordered structure, Intermetallics 18 (2010) 267–276.
[22] K. Hagihara, Y. Sugino, Y. Fukusumi, Y. Umakoshi, T. Nakano, Plastic deformation behavior of $Mg_{12}ZnY$ LPSO-phase with 14H-typed structure, Mater. Trans. 52 (2011) 1096–1103.
[23] S. Yoshimoto, M. Yamasaki, Y. Kawamura, Microstructure and mechanical properties of extruded Mg-Zn-Y alloys with 14H long period ordered structure, Mater. Trans. 47 (2006) 959–965.
[24] J.B. Hess, C.S. Barrett, Structure and nature of kink bands in zinc, Trans. Metall. Soc. AIME 185 (1949) 599–606.
[25] T. Itoi, T. Seimiya, Y. Kawamura, M. Hirohashi, Long period stacking structures observed in $Mg_{97}Zn_1Y_2$ alloy, Scr. Mater. 51 (2004) 107–111.
[26] W.B. Hutchinson, M.R. Barnett, Effective values of critical resolved shear stress for slip in polycrystalline magnesium and other hcp metals, Scr. Mater. 63 (2010) 737–740.